Effects of Submerged Convective Cooling In The Turning of AZ31 Magnesium Alloy For Tool Temperature And Wear Improvement

Muhammad Syamil Zakaria
Universiti Teknologi PETRONAS
Mazli Mustapha
Universiti Teknologi PETRONAS
Azwan Iskandar Azmi (aazm007@aucklanduni.ac.nz)
Universiti Malaysia Perlis https://orcid.org/0000-0002-9397-4458
Azlan Ahmad
Universiti Teknologi PETRONAS
Sikiru Oluwarotimi Ismail
University of Hertfordshire
Norshah Aizat Shuaib
Universiti Malaysia Perlis

Research Article

Keywords: Machinability, tool wear and tool temperature, magnesium alloy, internal cooling

Posted Date: September 22nd, 2021

DOI: https://doi.org/10.21203/rs.3.rs-875396/v1

Version of Record: A version of this preprint was published at The International Journal of Advanced Manufacturing Technology on March 2nd, 2022. See the published version at https://doi.org/10.1007/s00170-022-08985-9.

Abstract

Low melting point and material adhesion attributed by the magnesium alloy led to extreme built-up edge (BUE) and built-up layer (BUL) formations. Dry machining is favourable for machining magnesium alloy; however, this strategy inflicts excessive adhesive wear on the cutting tool. Therefore, this current work focuses on innovative cooling technique known as submerged convective cooling (SCC) for the turning of the AZ31 magnesium alloy. Prior to cutting experiment, a computational fluid dynamics (CFD) simulation was conducted to evaluate internal structure of cooling module. Based on the CFD simulation, small inlet/outlet diameter significantly contribute to reduction of tool temperature because of effective heat transfer coefficient of cooling fluid in the SCC. Experimental results revealed that SCC has effectively reduced the tool temperature by 50% and contributed to 37% improvement in surface roughness when compared to dry cutting. Finally, both BUE and BUL were observed in dry and SCC conditions, but the severity of these wear mechanisms improved or decreased remarkably under SCC conditions.

Introduction

Metal cutting is often associated with heat generation from the material compression at the primary shear zone as well as friction surfaces of the tool and workpiece at the secondary cutting zone. Consequent of high temperature or heat generation at these zones significantly influenced the tool wear mechanisms; namely, as abrasion, adhesion, diffusion, and built-up layer. Excessive amount of heat generated is a primary cause for accelerated tool wear that shorten tool useful life. In addition, heat conducted from the tool insert to the tool holder increases its temperature which compromises the dimensional accuracy and machined surface quality and integrity. Conventionally, cutting fluid is utilized as a key approach to metal removal, reduce temperature and facilitate heat transfer at the cutting zone as well as removing the chip from that zone [1, 2]. Presence of cutting fluids during machining process results in substantial improvement on cutting tool and workpiece. This is an excellent practice, as it alleviates the effects of friction on the tool flank face and the machined surface since cooling can be attained through dissipation and conduction of the generated heat. Thermal damage on workpiece material and cutting tools can be prevented through lubrication and cooling effect of the cutting fluid, consequently alleviating the tool wear [3].

Despite the key functions of cutting fluids for machining process improvement, it also has a few drawbacks as subsequently elucidated. Firstly, the cost associated with the procurement of the cutting fluids is as high as 16–30 % of the total manufacturing costs [4]. Secondly, due to the non-biodegradable nature of the fluids, expensive treatments prior to disposal are mandatory, which lead to high maintenance and disposal costs of up to two-folds of the cutting fluids purchasing costs [4, 5]. Thirdly, it has been reported that 80% of occupational skin diseases, respiratory ailments and cancer diseases among the machine operators were caused by inhalation of the cutting fluid [6]. Hence, the importance of sustainable manufacturing emerges to alleviate the aforementioned burden on the machining processes, environmental and their associated costs. This is where the dry cutting has a great advantage and can be a favorable option.

Dry cutting is an eco-friendly approach that assists in reducing harmful wastes and discharges. Elimination in the use of cutting fluids is possible through dry machining, hence, attributed to low processing cost and ecological hazard [7]. However, commercial and practical applications of dry machining are uncertain because of the absence of cooling and lubrication at tool-workpiece interface [8]. Excessive frictions at the tool- workpiece interfaces also trigger temperature rise that attributed to significant abrasion, diffusion and/or oxidation types of tool wear mechanisms. The reduction of tool sharpness hinders the achievement of close tolerances as there can be metallurgical damage on the workpiece superficial layer [7].

To compensate for the absence of cutting fluids or express the possibility of avoiding the use of cutting fluids, numerous studies have been undertaken. Encouraging approach would be through internal cooling, which included internal heat sinks, heat exchangers, vortex tubes and heat pipe [9–12]. Previously, researchers had proposed internal cooling tool by creating a cooling channel in the cutting tool to cool down tool temperature from underneath of the cutting insert [13–15]. In these designs, cooling fluids was able to decrease the tool temperature at its back. However, Hong SY et al. [16] discovered that the tool back cooling was less effective than cooling at tool rake face. This is because of the apparent distance between flank and the tool rake surfaces. Thus, it was suggested that the location of cooling source had close relationship with the cutting zone when determining the effectiveness of cooling strategy [15, 17]. Molinari et al. [18] reported a high thermal energy generation within the primary and secondary shear zones. Temperature profile has depicted a hot spot at the rake face and the generated heat intensity was subjected to specific workpiece deformation. Therefore, it is important to accurately locate the cooling source near to the cutting edges to revoke the insert's low thermal conductivity.

Meanwhile, magnesium alloys have received a great interest recently, because of its useful in several applications; namely, automotive, aerospace, microelectronics, and most lately in bio-medical applications. The recent uses of magnesium alloys in bio-medical industries can be attributed to their superior biodegradable properties and corrosion resistant [19]. However, their low melting point contributed to ignition of the chips when machining temperature exceeds 450 ^{o}C [8]. As a result, the use of cooling fluids is needed during machining of magnesium alloys for proper cutting temperature controlled. However, problem occurs when water-based coolant is applied during machining of magnesium alloys, because the reaction of water to magnesium alloys produces hydrogen gas that can lead to an explosion. To minimize this risk, dry cutting is favorable in cutting magnesium alloy, but suitable cutting parameter must be properly determined to ensure cutting process is conducted below critical temperature to avoid fire hazard, especially at elevated cutting speed.

Despite of widely established study on indirect cooling, there are limited research focusing on indirect cooling for machining light weight alloys especially on magnesium alloy. Most of previous studies are mainly devoted on cutting titanium alloy and nickel-based alloy [9, 13, 15]. Besides, there is still lack of study in tackling adhesion wear mechanism such as BUE and BUL by using indirect cooling. Therefore, in this study, an innovative and sustainable technique of submerged convective cooling (SCC) was introduced by partially submerged the tool rake face into a cooling medium to reduce tool temperature via

internal cooling. Performance of the SCC was evaluated based on the capability of its heat removal, effect on cutting temperature and tool wear mechanism.

Submerged Convective Cooling (Scc) Tool

Figure 1 presents a submerged convective cooling (SCC) tool, which is considered as one of indirect cooling technique for cutting tool during machining. According to Hong S.Y. et al. [16], cooling at the rake face has a profound influence for temperature reduction instead of cooling the tool back. Therefore, in the design of SCC tool, the fluid enters the cooling module from the top of rake face and pass-through the rake face before leaving out to the outlet. Re-circulating fluids inside the cooling module dissipate heat from the cutting insert via convection principle through the rake face. At the contact interface between cooling module and rake face, silicon gasket was applied to seal the fluid from any leak and to avoid water contact with magnesium alloy. This cooling module was specially designed and fabricated from aluminum alloy to create a partially enclosed rake face while the remaining is utilized for cutting operation as shown in Fig. 2.

Since the maximum temperature is near the cutting edge, thus, the cooling source must be located near to the cutting edge. No modification was done on the cutting tool to ensure that the integrity of the insert structure and the tool remain intact. The SCC module was attached to an uncoated carbide insert CNMA120408, which was mounted on a standard tool holder PCLNLK202012 from Mitsubishi. Tool holder has an entering angle of 95^{o}, rake angle and inclination angle of -6^{o}. The completed circuit of SCC set-up is shown in Fig. 3. The cooling circuit consists of pump, tank, flow meter and cooling module was connected to each other by hose and fittings. Water was used as the cooling fluid due to its efficiency and pronounced cooling ability. Besides, water does not require much treatment during disposal and could be used for a long time. Cooled water was stored in a tank, and it was pumped into the cooling module using a DC water pump at 1 L/min pumping rate.

2.1 Design of Internal Structure of Cooling Module

The unique component of the SCC tool is the assembly of cooling module. It consists of clamper, fixing screw, cooling module, inlet, and outlet barb fitting. A clamper was used to press the cooling module tightly and securely on the insert rake face. Fixing screw was used to ensure cooling module can be firmly attached to the cutting insert. On top of the cooling module, inlet barb was fitted by a screw thread while inside the cooling module, a cavity was milled to accommodate the incoming cooling fluid. At the back, outlet barb was also fitted by screw thread. To avoid cooling fluid leakage, a groove was created to fit a silicon gasket around the cavity area. The narrow space of the turning machined area can constrain the overall dimension of cooling structure, in which this condition has affected the height, H of cooling module as well as the cavity depth, *d* as shown in Fig. 4. H was fixed at 16 mm, since this was the maximum allowable height before it interfered the workpiece being machined. The cavity depth, *d* was set as 5 mm, taking into consideration of possibility of fluid leakage. Prior to the simulation, inlet/outlet diameter ranges were decided based on working condition of the entire SCC tool system. As SCC tool

system was designed to operate safely at designated flow rate, diameter range was determined to be around 3–7 mm. It is to note that a very low inlet diameter would lead to over pressurized fitting that may lead to fluid leakage.

2.1.1 Numerical analysis of SCC tool thermal performance

Prior to experimental work, optimum dimension of inlet/outlet diameter with varying the flow rate was determined based on the maximum tool temperature. The optimisation of the diameter was facilitated via ANSYS Fluent, a commercially available computational fluid dynamics (CFD) software. The software package was applied to resolve the thermal model of the SCC tool. CFD analysis is actively utilized in engineering application including in metal cutting field [20–22]. Table 1 depicts the material properties used in the CFD simulation.

Table 1
Material properties for CFD simulation.[23][24]

Parameters	Insert	Cooling Module (Aluminum alloy)	Water	Air
Density (kg/m^3)	15000	2719	1000	
Thermal conductivity (W/m.K)	46	202	0.6	
Specific heat capacity (J/kg.K)	203	871	4200	
Water temperature (^{o}C)			20	
Viscosity of water (kg/m.s)			0.001	
Flow rate (ml/min)			50,90,130	
Heat transfer coefficient (W/m^2.K)				5
Air temperature (^{o}C)				27

Three-dimensional CFD model was developed to assess cooling capacity of the SCC tool based on the inlet/outlet diameter of the cooling module. Simulation of flow field was employed to examine the effect of inlet/outlet diameter of SCC tool on the velocity and the cooling fluid convective heat transfer coefficient, as depicted in Fig. 5. The following boundary conditions of the model were specified; (1) Fluid inlet was defined as mass flow inlet, (2) pressure and temperature were set to an atmospheric pressure and 27^{o}C respectively, for the fluid outlet. Rest of SCC tool surfaces except A_c, cooling area and A_{tc}, tool chip contact area were set expose to surrounding air.

In conducting the simulation, a full factorial test was implemented for independent variables of inlet/outlet diameter and flow rate as depicted in Table 2. Fluid flow inside the cooling module establish a force convection from the motion of fluid to absorb heat from cutting tool. The amount of heat flowing to

the cooling fluid and the heat dissipation from the Newton law of cooling can be calculated based on Eq. (1) and Eq. (2) respectively.

$$\dot{Q} = \dot{m} c_p (T_{out} - T_{in}) \quad (1)$$

$$\dot{Q} = h\, A_c (T_s - T_f) \quad (2)$$

where $\dot{m}$, c_p, T_{out}, and T_{in} are mass flow rate, specific heat capacity of fluid, outlet temperature and inlet temperature and h is convective heat transfer coefficient, A_c is cooling area, T_s is insert temperature and T_f is the mean fluid temperature. Before commencing the CFD analysis, the heat flux generated at tool – chip contact area was determined based on experimental tool temperature. Once the heat flux has been finalized, a parametric study on the inlet/outlet diameter was carried out using the CFD analysis to determine optimum geometry of the final design configuration of the cooling module. Laminar model was adopted to simulate the flow field inside the cooling module. The flow rate employed in this study were determined to be in laminar flow states based on Reynolds number, Re as given by Eq. (3):

$$Re = \frac{\rho V D}{\mu} \quad (3)$$

where ρ,V,D and μ are the density, inlet velocity, inlet diameter and dynamic viscosity respectively.

Table 2
Simulation parameters.

Parameter	Value
Inlet/Outlet diameter (mm)	3, 4, 5, 6, 7
Flow rate (ml/min)	50, 90, 130

Material And Methods

3.1 Workpiece material

The received AZ31 magnesium alloy cylinder rods of 30 mm diameter were cut into a 100 mm length. However, only a length of 50 mm was utilized for cutting in each pass to avoid chattering. The chemical composition of work material is presented in Table 3.

Table 3
Chemical composition of the AZ31 magnesium alloy bar.

Chemical composition (wt %)							
Material	Mg	Al	Zn	Mn	Si	Fe	Ca
AZ31	Bal	3.1	0.73	0.25	0.02	0.005	0.0014

3.2 Cutting trials

Cutting experiment was conducted using a CNC Turning T6 Compact Quicktech, considering both dry and SCC conditions, as shown in Fig. 6. Machining parameter was kept constant: cutting speed (V_c), depth of cut (a_p) and feed rate (f) were 120 m/min, 1 mm and 0.1 mm/rev, respectively. Also, flow rates of the coolant or water were varied, as: 50, 90 and 130 ml/min. Cooled water with temperature constantly at 20 ^{o}C was stored in the tank to act as cooling fluid. Rake face temperature distribution was recorded for each cutting condition.

3.3 Temperature measurement

A thermal imaging camera, FLIR T440, was utilized to locate the hot spot and temperature distribution on the rake face and chip. The FLIR Tools software was installed in the computer to dynamically display the infrared images. The camera has spectral range of 7.5 to 13 µm, a frame rate of 60 Hz and thermal sensitivity of 0.045 ^{o}C at 30 ^{o}C. Thermal imaging camera was located 300 mm above the rake face, as shown in Fig. 6(a). The emissivity of uncoated carbide insert was determined at 0.7 by heating it from 50 to 400 ^{o}C and 0.18 for AZ31 Mg alloy [25].

3.4 Wear, tool chip contact length and surface roughness measurement

Wear and element analyses on the magnesium alloy material and tool were carried out using a scanning electron microscopy (SEM) JEOL JSM-6010LV and energy dispersive spectroscopy (EDS) after 30 minutes of cutting, respectively. Subsequently, surface roughness, was determined at four locations on every sample and average reading was taken as an arithmetic average, R_a using surface roughness Mitutoyo SJ-410 tester. The test was conducted according to ISO 4287 standard. The tool chip contact length was observed and measured by Xoptron X80 series of high-power optical microscopy identified by using the contact tracks left by the chip on the tool rake face.

Results And Discussion

4.1 Simulation results

4.1.1 Tool-chip contact area and heat flux

Initially, dry cutting was conducted to determine the heat flux and tool-chip contact area for input parameters of the simulation. Based on dry cutting experiment, the maximum tool temperature and tool chip contact area, A_{tc} (L_c x a_p) were determined to be 86.3 ^oC and (0.4 mm x 1 mm), respectively. An arbitrary value of heat flux was applied to the tool chip contact area in the numerical model. Subsequently, iteration steps were taken as a procedure to attain the absolute accurate value of the heat flux, which was 2.1 x 10^6 W/m^2. The result was validated with the experimental data based on the maximum tool temperature, as shown in Fig. 7.

4.1.2 Effect of inlet/outlet diameter and flow rate

Maximum tool temperature in the SCC tool was plotted in Fig. 8. In general, tool temperature was proportionally increased with the inlet/outlet diameter. Lowest tool temperatures were obtained with the 3 mm inlet/outlet diameter for each respective flow rate. Most importantly, variation in the tool temperature was marginal as the diameter was changed from 3 mm to 7 mm. For instance, the tool temperature has declined by only 0.5 ^oC for the flow rate of 50 mL/min. On the other hand, the tool temperature has depicted a downward trend as the flow rate has changed from 50 ml/min to 130 ml/min.

Temperature gradient of the cutting tool is shown in Fig. 9, which depicting the cooling effect from the cooling fluid or fluid flow. It is apparent that the highest temperature was concentrated at tool tip, whereas the rest of the tool surfaces have maintained a room temperature gradient.

Maximum tool temperature was strongly influenced by the heat transfer coefficient of the cooling fluid as illustrated in Fig. 10. Heat transfer coefficient of cooling fluid was extracted from location A_c, cooling area of the simulation. High heat transfer coefficient implies greater high dissipation from the cutting tool. It is apparent that the highest heat transfer coefficient was produced by the 3 mm inlet/outlet diameter for each respective flow rate, and it declined gradually with the increasing inlet/outlet diameter.

According to Cengel [26], fluid velocity greatly influences the convective heat transfer coefficient in forced convection. With this respect, the effects of inlet/outlet diameter to fluid velocity and the percentage reduction of fluid velocity for respective diameter and flow rate are depicted in Fig. 11. The highest fluid velocity was recorded when the inlet/outlet diameter was 3 mm for each set of flow rate, and it continued to drop with larger inlet/outlet diameter. Therefore, 3 mm diameter of the inlet attributed to the highest heat transfer coefficient as illustrated in Fig. 10.

Meanwhile, the reduction of fluid velocity was analyzed as shown in Fig. 11. This is a vital indicator to ensure that the fluid velocity remains at its highest velocity. From Fig. 11, regardless of the fluid flows, the loss of fluid velocity grew as the inlet/outlet diameter increased. 3 mm inlet/ outlet diameter recorded the least loss of velocity for each set of flow rate with the minimum loss of 15% for a flow rate of 130 ml/min. Based on the simulations, it can be concluded that effective convective heat transfer coefficient can lead to a low tool temperature. The highest heat transfer coefficient was obtained when the inlet/outlet diameter was 3 mm, and it has maintained an upward trend with the flow rate. Considering all these factors (inlet velocity and tool temperature) into account, SCC tool had a pronounced cooling

performance when the inlet/outlet diameter was 3 mm. Thus, the optimum dimension of inlet/outlet diameter was confirmed, and the actual fabricated SCC tool is shown in Fig. 12.

4.2 Heat distribution on rake face

Thermal imaging aids the identification of the hot spot and analysis of the heat distribution on the rake face when exposed to heat generated from cutting process. Thermal image at rake face was captured immediately at end stroke of cutting. To avoid interruption from the chip and workpiece, the tool was retracted from the workpiece prior to capturing the image. As shown in Fig. 13, there was significance drop in tool temperature, but a nearly similar chip temperature of AZ31 magnesium alloy was obtained. Figure 14 shows thermal distribution on the rake face after 1 minute of cutting for both dry and SCC conditions. There was a significant reduction on the tool rake face temperature from dry to SCC condition at 130 ml/min; precisely from 86.3 to 42.1 ^{o}C, as shown in Figs. 14(a) and (d), respectively.

This reduction or improvement was roughly 50%. Evidently, the effect of flow rate in SCC condition showed a downtrend in tool temperature, yet the difference was minor and between 1 to ~ 5 ^{o}C, as captured and presented in Figs. 14(b)-(d). Low thermal conductivity of uncoated tungsten carbide might have hindered the heat transfer from the tool to the cooling fluid even though the flow rate was raised. Minton et al. [15] had discovered that the uncoated tool conducted heat slower than diamond coated tool in cutting titanium alloy by internal cooling system, due to low thermal conductivity.

Moreover, it was observed in dry condition that the heat distribution was spreading all over the rake face as well as to the cutting tool. However, the highest temperature was spotted slightly away from the cutting edge; the area where the chip had contact with the tool. In contrast, for SCC condition, the heat was maintained near the tool tip without heating up the entire tool, with less peak temperature generated. Since a lower feed rate was employed in this study, the contribution of heat at the rake face was mainly originated from the sliding chip [27]. Therefore, it was understood that the heat source was moving towards the cooling source for SCC condition. Besides, it has been established in cutting simulation that maximum temperature occurred at 0.4 mm away from the cutting edge and the heat flux flowed into the tool along the entire contact region [28]. Consequently, tool temperature was reduced in SCC condition. This was in agreement the investigation conducted by Minton et al. [15] and Wu et al. [29]. They reported that internally cooled tool significantly exhibited a reduction in its temperature.

In metal cutting, 70 to ~ 80% of heat generated is carried away by the chip. Figure 15 shows the temperature variation of chip for different machining conditions. Dry condition produced chip temperature of 248.3 ^{o}C, whereas lowest chip temperature of 230 ^{o}C was recorded with SCC condition at flow rate of 130 ml/min. This decrease or enhancement was approximately 8%. The variation of chip temperatures between dry and SCC conditions was not much or smaller, when compared with that of tool temperature. This phenomenon did not imply ineffectiveness of submerged cooling, instead it was a consequence of enormous heat reduction in the tool. This was evidently demonstrated by Ozel [30], in which the reduction of 180 ^{o}C at tool-chip interface temperature led to 30 ^{o}C decrease in chip temperature. Besides, the observed low deviation of the chip temperature established the fact that

frictional heat was evacuated by the chip instead of conducted to the tool, as this can be linked to high chip velocity [31].

4.3 Contact length, chip formation and tool wear mechanisms

Effects of cutting conditions and flow rates on tool-chip contact length were investigated and discussed in this sub-section. As shown in Fig. 16, higher value of tool – chip contact length of 0.415 mm was recorded in dry condition when compared with SCC with an average value of 0.300 mm, resulting to nearly 28% reduction. This occurrence can be related to that of tool and chip temperatures, as previously explained. Long contact length implied larger contact area and high stress between chip and tool. Thus, enormous amount of heat generated at tool – chip interface, caused by friction was absorbed by the tool [32, 33].

Considering Fig. 17, chip produced in dry condition was continuous type, which was coincidental to tool temperature and contact length. Nevertheless, in the SCC system/condition, a downtrend in tool-chip contact length was depicted. With higher flow rate, the tool-chip contact length was reduced. This is an indication that the cooling had significant effect on the tool – chip contact length. At lowest flow rate of 50 ml/min, contact length was 0.33 mm, while maximum flow rate of 130 ml/min reduced contact length to 0.25 mm. Tasdelen et al. [34] A reported a similar outcome in which minimum quantity lubrication (MQL) and compressed air recorded comparable total contact length, due to chip-up curling caused by the cooling effect.

High flow rate provides more heat absorption, which was evidently shown by tool and chip temperatures (Fig. 13). The low tool-chip contact length produced discontinuous and shorter chips, as depicted in Fig. 10. Besides, the structure of the cooling module incorporated on the rake face indirectly contributed to the low contact length. The structure of SCC system created an obstruction to the chip, which forced the chip to curl up similar to that of cutting tool with chip breaker.

Furthermore, built-up layer (BUL) is commonly observed during machining of Mg alloy [35–37]. BUL is a kind of adhesion wear mechanism in metal cutting that is thermally sensitive, especially to workpiece-tool temperature [38]. This particular wear mechanism always occurs at high temperature and is very difficult to prevent [39]. The zone where heat is absorbed by either the cutting edge or flank face is identified favorable location of BUL formation. The phenomenon of flank built-up (FBU) during cutting of magnesium alloy is associated to low melting temperature of around 618 ^{o}C, thus the material tends to weld on the tool rake face. Presence of both manganese (Mn) and aluminum (Al) compounds in the BUL area has been identified as the key factors responsible for adhesion mechanism in cutting Mg alloy, as it has high affinity with tool materials [35].

Moving forward, the results from the chemical analysis conducted using EDS are shown in Fig. 18. It was evidently observed in both conditions that there were presence of Mn and Al elements on the rake face. In this current study, both build-up edge (BUE) and FBU were observed in both dry and SCC cutting

conditions. However, the severity of BUE and FBU were different. With dry condition, both BUE and FBU produced were worse. But the severity of these wear mechanisms improved or decreased tremendously with SCC condition. SEM image in Fig. 19 shows BUE at the cutting edge and FBU on the rake face. They were intensified in dry condition, due to high cutting temperature. It can be further explained that the plastic deformation of the workpiece material in primary zone generated enormous heat closed to cutting edge, therefore it caused melted AZ31 magnesium alloy to adhere on the cutting edge. The significant formation of FBU observed on the tool rake face in dry condition was attributed to the rapid heat growth, due to the friction effect between chip and tool.

On the other hand, cutting with SCC provided a cooling effect on the tool. With the presence of cooling effect, cutting process occurred below the critical temperature. Hence, the melting temperature of AZ31 magnesium alloy was delayed at the cutting edge. However, friction between the chip and tool raised the temperature rapidly as the chip flowed on the rake face. This led to workpiece material adhesion on the tool rake face, but it was immensely improved in SCC condition with clean surface observed on the tool face, as shown in Fig. 19.

Surface roughness possesses great influence on the final quality of workpiece material. In case of AZ31 magnesium alloy, smoothen surface roughness can improve its corrosion resistance [40]. From Fig. 20, surface roughness was improved under SCC condition when compared with dry condition. Surface roughness in SCC decreased or improved by nearly 37% in comparison with dry cutting. A better surface roughness in SCC can be mainly attributed to the reduction in temperature at cutting zone, thus decreasing the melting of AZ31 magnesium alloy on machined surface and cutting edge. This was similarly reported on cryogenic cutting of magnesium alloy, where surface roughness was improved due to cooling effect [25]. However, in SCC with increasing flow rate, surface roughness showed no improvement and it maintained value of around 0.151 μm. Also, surface roughness was deteriorated to 0.178 μm with SCC at maximum feed rate of 130 ml/min., due to irregular flow of chips and consequence of uneven BUE formation along the cutting edge.

Conclusions

In this study, innovative and sustainable cooling technique via submerged convective cooling was proposed. The technique proposed environmentally friendly machining strategy using water as a coolant and suppressed usage of other mineral based fluids. The effects of using the technique were investigated and analyzed on both tool and chip/workpiece. Dry turning machining/cutting was conducted and compared with the effectiveness of SCC condition with respect to tool wear, temperature, chip contact length and surface finish of AZ31 magnesium alloy material. Based on experimental results obtained, the following concluding remarks can be drawn:

- CFD simulation revealed that small inlet/outlet diameter of 3 mm significantly contributed to tool temperature reduction because of effective heat transfer coefficient of the SCC.
- SCC condition significantly reduced tool and chip temperatures by 50% and 8% respectively, when compared to the dry cutting condition. Slight variation was obtained at both maximum tool and chip

temperatures with an increasing flow rate in SCC.

- Tool-chip contact length obtained from SCC was superior by 28% to that of dry cutting condition, implying consequence of cooling effect from the sustainable cooling fluid perspective. High flow rate produced less tool and chip contact lengths, which led to low temperature of the cutting tool.
- Both BUE and FBU were observed in SCC and dry cutting conditions. However, severity of both turning-induced damage profoundly improved or reduced in SCC condition, due to delay in melting of AZ31 magnesium alloy. This was significantly attributed to the presence of cooling fluid from SCC condition.
- As BUE and FBU were reduced in SCC, surface finish of AZ31 magnesium alloy was decreased by nearly 37%, when compared with dry cutting condition. This was a notable improvement, as some performance properties and fracture of many components depend on their surface roughness values.

Declarations

Funding: This work was supported by Ministry of Higher Education, Malaysia under the grant number of FRGS/1/2020/TK0/UNIMAP/03/15.

Competing/ Conflicts of interest: The authors declare no competing interests.

Availability of data: Data is available with the permission of Universiti Malaysia Perlis. The data that support the findings of this study are available from the corresponding author upon reasonable request.

Code availability: Not applicable

Ethical approval: This research work does not contain any studies with human participants or animals performed by any of the authors.

Consent to participate: Not applicable.

Consent for publication: The authors declare that they all consent and approved for the publication.

Author contributions:

Conceptualization: Mazli Mustapha, Azwan Iskandar Azmi and Azlan Ahmad;

Methodology and Investigation: Muhammad Syamil Zakaria, Azwan Iskandar Azmi and Mazli Mustapha;

Writing, validation and Visualization: Muhammad Syamil Zakaria, Azwan Iskandar Azmi, Mazli Mustapha, Sikiru Oluwarotimi Ismail and Norshah Aizat Shuaib;

Supervision: Mazli Mustapha, Azwan Iskandar Azmi, Azlan Ahmad.

Acknowledgements We are grateful and thank to the Ministry of Higher Education, Malaysia for the financial support received under the Fundamental Research Grant Scheme (FRGS) with the grant number of FRGS/1/2020/TK0/UNIMAP/03/15.

References

1. Şirin Ş, Yıldırım ÇV, Kıvak T, Sarıkaya M (2021) Performance of cryogenically treated carbide inserts under sustainable cryo-lubrication assisted milling of Inconel X750 alloy. Sustain Mater Technol 29:e00314. https://doi.org/10.1016/j.susmat.2021.e00314
2. Sharif MN, Pervaiz S, Deiab I (2016) Potential of alternative lubrication strategies for metal cutting processes: a review. Int J Adv Manuf Technol 89:2447–2479. https://doi.org/10.1007/S00170-016-9298-5
3. Brinksmeier E, Meyer D, Huesmann-Cordes AG, Herrmann C (2015) Metalworking fluids—Mechanisms and performance. CIRP Ann 64:605–628. https://doi.org/10.1016/j.cirp.2015.05.003
4. Debnath S, Reddy MM, Yi QS (2014) Environmental friendly cutting fluids and cooling techniques in machining: A review. J Clean Prod 83:33–47. https://doi.org/10.1016/j.jclepro.2014.07.071
5. Shokrani A, Dhokia V, Newman ST (2012) Environmentally conscious machining of difficult-to-machine materials with regard to cutting fluids. Int J Mach Tools Manuf 57:83–101. https://doi.org/10.1016/j.ijmachtools.2012.02.002
6. Chetan GS, Venkateswara Rao P (2015) Application of sustainable techniques in metal cutting for enhanced machinability: A review. J Clean Prod 100:17–34. https://doi.org/10.1016/j.jclepro.2015.03.039
7. Diniz AE, Micaroni R (2002) Cutting conditions for finish turning process aiming: the use of dry cutting. Int J Mach Tools Manuf 42:899–904. https://doi.org/10.1016/S0890-6955(02)00028-7
8. Goindi GS, Sarkar P (2017) Dry machining: A step towards sustainable machining e Challenges and future directions. J Clean Prod 165:1557–1571. https://doi.org/10.1016/j.jclepro.2017.07.235
9. Vicentin GC, Sanchez LEA, Scalon VL, Abreu GGC (2011) A sustainable alternative for cooling the machining processes using a refrigerant fluid in recirculation inside the toolholder. Clean Technol Environ Policy 13:831–840. https://doi.org/10.1007/s10098-011-0359-z
10. Liang L, Quan Y, Ke Z (2011) Investigation of tool-chip interface temperature in dry turning assisted by heat pipe cooling. Int J Adv Manuf Technol 54:35–43. https://doi.org/10.1007/s00170-010-2926-6
11. Zhao H, Barber GC, Zou Q, Gu R (2006) Effect of internal cooling on tool-chip interface temperature in orthogonal cutting. Tribol Trans 49:125–134. https://doi.org/10.1080/05698190500544163
12. Liu J, Kevin Chou Y (2007) On temperatures and tool wear in machining hypereutectic Al-Si alloys with vortex-tube cooling. Int J Mach Tools Manuf 47:635–645. https://doi.org/10.1016/j.ijmachtools.2006.04.008

13. Isik Y (2016) Using internally cooled cutting tools in the machining of difficult-to-cut materials based on Waspaloy. Adv Mech Eng 8:1–8. https://doi.org/10.1177/1687814016647888
14. Sanchez LEDA, Neto RRI, Fragelli RL, Junior CEDS, Scalon VL (2016) Machining with Internally Cooled Toolholder Using a Phase Change Fluid. Procedia CIRP 41:847–851. https://doi.org/10.1016/j.procir.2015.12.007
15. Minton T, Ghani S, Sammler F, Bateman R, Fürstmann P, Roeder M (2013) Temperature of internally-cooled diamond-coated tools for dry-cutting titanium. Int J Mach Tools Manuf 75:27–35. https://doi.org/10.1016/j.ijmachtools.2013.08.006
16. Hong SY, Markus I, Jeong W (2001) New cooling approach and tool life improvement in cryogenic machining of titanium alloy Ti-6Al-4V. Int J Mach Tools Manuf 41:2245–2260. https://doi.org/10.1016/S0890-6955(01)00041-4
17. Huang S, Lv T, Wang M, Xu X (2018) Effects of Machining and Oil Mist Parameters on Electrostatic Minimum Quantity Lubrication–EMQL Turning Process. Int J Precis Eng Manuf - Green Technol 5:317–326. https://doi.org/10.1007/s40684-018-0034-5
18. Molinari A, Cheriguene R, Miguelez H (2012) Contact variables and thermal effects at the tool–chip interface in orthogonal cutting. Int J Solids Struct 49:3774–3796. https://doi.org/10.1016/j.ijsolstr.2012.08.013
19. Chen J, Tan L, Yu X, Etim IP, Ibrahim M, Yang K (2018) Mechanical properties of magnesium alloys for medical application: A review. J Mech Behav Biomed Mater 87:68–79. https://doi.org/10.1016/j.jmbbm.2018.07.022
20. Pervaiz S, Deiab I, Wahba E, Rashid A, Nicolescu CM (2015) A novel numerical modeling approach to determine the temperature distribution in the cutting tool using conjugate heat transfer (CHT) analysis. Int J Adv Manuf Technol 80:1039–1047. https://doi.org/10.1007/s00170-015-7086-2
21. Fang Z, Obikawa T (2020) Influence of cutting fluid flow on tool wear in high-pressure coolant turning using a novel internally cooled insert. J Manuf Process 56:1114–1125. https://doi.org/10.1016/J.JMAPRO.2020.05.028
22. Pervaiz S, Deiab I, Wahba E, Rashid A, Nicolescu M (2018) A numerical and experimental study to investigate convective heat transfer and associated cutting temperature distribution in single point turning. Int J Adv Manuf Technol 94:897–910. https://doi.org/10.1007/s00170-017-0975-9
23. Yvonnet J, Umbrello D, Chinesta F, Micari F (2006) A simple inverse procedure to determine heat flux on the tool in orthogonal cutting. Int J Mach Tools Manuf 46:820–827. https://doi.org/10.1016/J.IJMACHTOOLS.2005.07.030
24. Özel T, Zeren E (2007) Finite element modeling the influence of edge roundness on the stress and temperature fields induced by high-speed machining. Int J Adv Manuf Technol 35:255–267. https://doi.org/10.1007/s00170-006-0720-2
25. Danish M, Ginta TL, Habib K, Carou D, Rani AMA, Saha BB (2017) Thermal analysis during turning of AZ31 magnesium alloy under dry and cryogenic conditions. Int J Adv Manuf Technol 91:2855–2868. https://doi.org/10.1007/s00170-016-9893-5

26. Çengel Y (2020) Heat and mass transfer: fundamentals & applications. McGraw-Hill Education, New York
27. Mane S, Joshi SS, Karagadde S, Kapoor SG (2020) Modeling of variable friction and heat partition ratio at the chip-tool interface during orthogonal cutting of Ti-6Al-4V. J Manuf Process 55:254–267. https://doi.org/10.1016/j.jmapro.2020.03.035
28. Lazoglu I, Altintas Y (2002) Prediction of tool and chip temperature in continuous and interrupted machining. Int J Mach Tools Manuf 42:1011–1022. https://doi.org/10.1016/S0890-6955(02)00039-1
29. Wu T, Li T, Ding X, Chen H, Wang L (2018) Design of a Modular Green Closed Internal Cooling Turning Tool for Applications. Int J Precis Eng Manuf - Green Technol 5:211–217. https://doi.org/10.1007/s40684-018-0021-x
30. Özel T (2006) The influence of friction models on finite element simulations of machining. Int J Mach Tools Manuf 46:518–530. https://doi.org/10.1016/j.ijmachtools.2005.07.001
31. Haddag B, Atlati S, Nouari M, Zenasni M (2015) Analysis of the heat transfer at the tool–workpiece interface in machining: determination of heat generation and heat transfer coefficients. Heat Mass Transf 51:1355–1370. https://doi.org/10.1007/s00231-015-1499-1
32. Iqbal SA, Mativenga PT, Sheikh MA (2009) A comparative study of the tool-chip contact length in turning of two engineering alloys for a wide range of cutting speeds. Int J Adv Manuf Technol 42:30–40. https://doi.org/10.1007/s00170-008-1582-6
33. Azizur Rahman M, Rahman M, Senthil Kumar A (2018) Influence of relative tool sharpness (RTS) on different ultra-precision machining regimes of Mg alloy. Int J Adv Manuf Technol 96:3545–3563. https://doi.org/10.1007/S00170-018-1599-4
34. Tasdelen B, Thordenberg H, Olofsson D (2008) An experimental investigation on contact length during minimum quantity lubrication (MQL) machining. J Mater Process Technol 203:221–231. https://doi.org/10.1016/j.jmatprotec.2007.10.027
35. Tomac N, Sørby K, Doboviček S (2018) Formation of built-up layer on the tool in turning Operation of Magnesium Alloys. Tech Gaz 25(3):940–943. https://doi.org/10.17559/TV-20151027130036
36. Shi K, Ren J, Zhang D, Zhai Z, Huang X (2017) Tool wear behaviors and its effect on machinability in dry high-speed milling of magnesium alloy. Int J Adv Manuf Technol 90:3265–3273. https://doi.org/10.1007/s00170-016-9645-6
37. Cagan SC, Buldum BB, Özkul İ (2019) Chip morphology in turning of AZ91D magnesium alloy under different machining conditions. J Nat Appl Sci 23:119–125. https://doi.org/10.19113/sdufenbed.443411
38. Gåård A, Hallbäck N, Krakhmalev P, Bergström J (2010) Temperature effects on adhesive wear in dry sliding contacts. Wear 268:968–975. https://doi.org/10.1016/j.wear.2009.12.007
39. Sharma VS, Dogra M, Suri NM (2009) Cooling techniques for improved productivity in turning. Int J Mach Tools Manuf 49:435–453. https://doi.org/10.1016/j.ijmachtools.2008.12.010

40. Uddin M, Hall C, Hooper R, Charrault E, Murphy P, Santos V (2018) Finite Element Analysis of Surface Integrity in Deep Ball-Burnishing of a Biodegradable AZ31B Mg Alloy. Metals 8(2):136. https://doi.org/10.3390/met8020136

Figures

Figure 1

(a) Assembly of SCC tool (b) Circulating fluid inside the cooling module.

Figure 2

Definition of effective surface on the tool rake face.

Figure 3

SCC tool circuit

Figure 4

(a) Cooling module (b) Section view C-C.

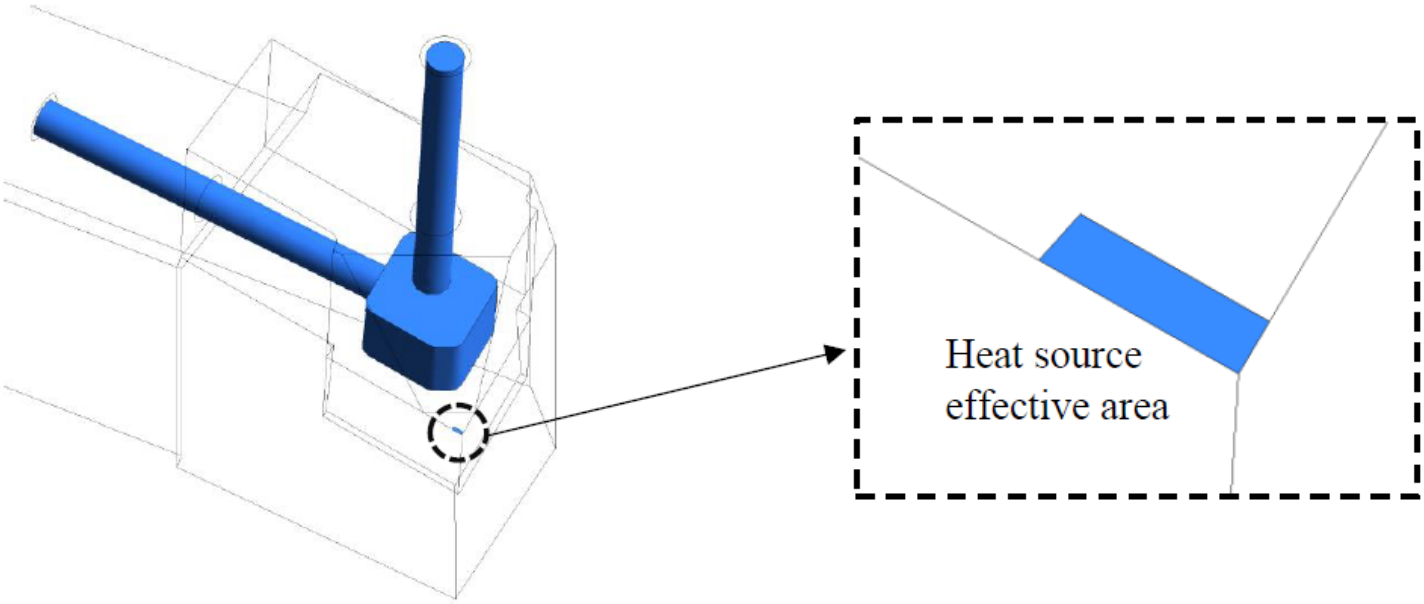

Figure 5

Fluid domain and heat boundary in SCC tool.

Figure 6

Machining set-up for (a) dry cutting and (b) SCC conditions.

Figure 7

Comparison of maximum tool temperature in dry cutting for experiment and simulation.

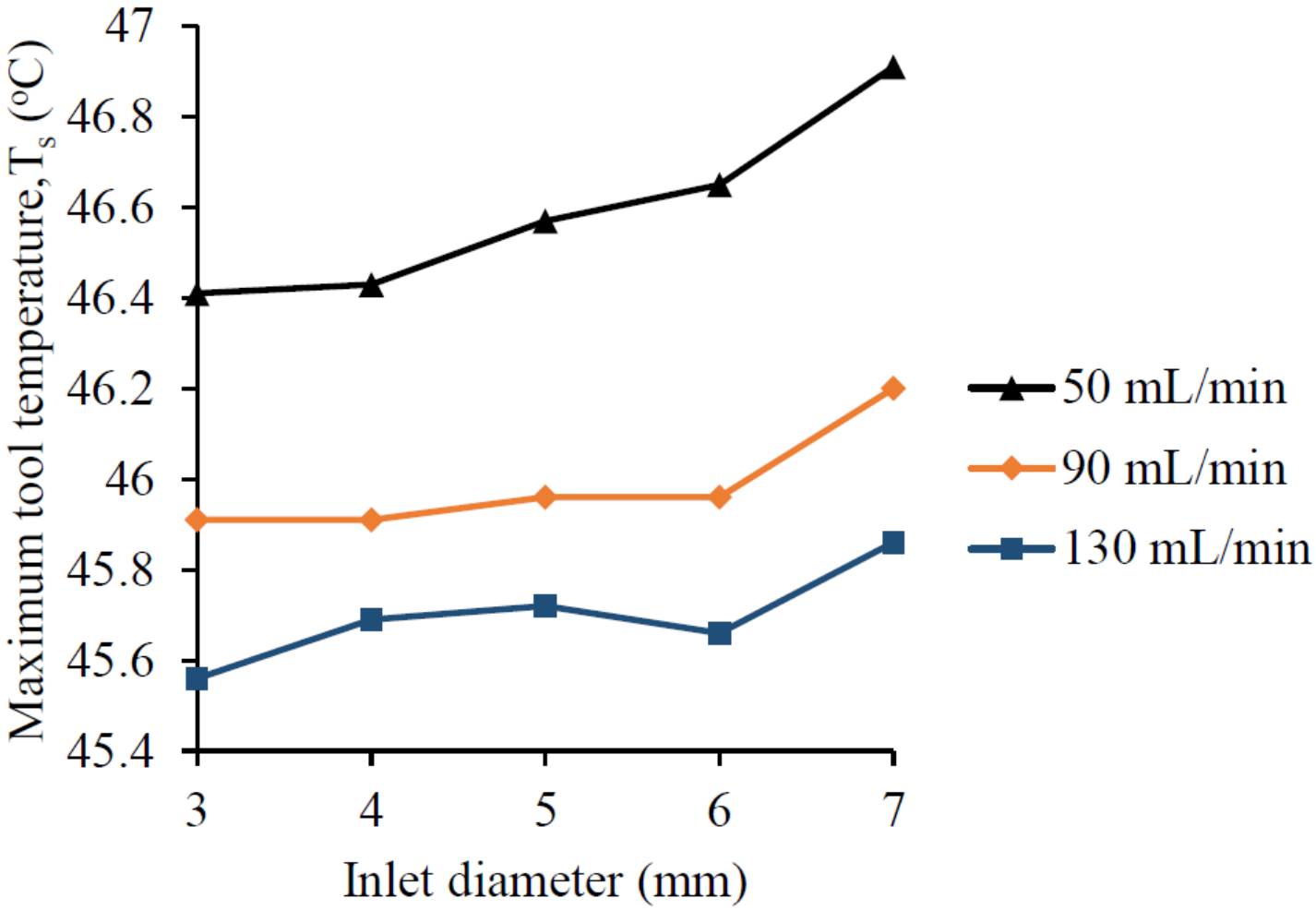

Figure 8

Maximum tool temperature in the SCC tool.

Figure 9

Temperature contour of SCC tool (Ø=3 mm,$\dot{m}$ = 130 mL/min).

Figure 10

Heat transfer coefficient of cooling fluid.

Figure 11

Influence of inlet/outlet diameter on reduction of fluid velocity at flow rates of (a) 50 ml/min (b) 90 ml/min (c) 130 ml/min.

Figure 12

Actual SCC tool.

Figure 14

Thermal image at maximum tool temperature during: (a) dry, SCC conditions at (b) 50, (c) 90 and (d)130 ml/min flow rates.

Figure 15

Thermal image at maximum chip temperature of AZ31 magnesium alloy during (a) dry as well as SCC conditions at (b) 50, (c) 90 and (d) 130 ml/min flow rates.

Figure 16

Definition of effective surface on the tool rake face.

Figure 17

Chip formation and tool-chip contact length for different flow rates.

Figure 18

EDS spectrum on tool flank face during (a) dry cutting and (b) SCC at flow rate of 130 ml/min.

Figure 19

Formation of BUE and BUL on tool rake face during (a) dry and (b)-(d) different SCC flow rates.

Figure 20

Surface roughness of AZ31 magnesium alloy under at different flow rates.